Indian Journal of Pure & Applied Physics
Vol. 58, June 2020, pp. 470-477

Performance of ZnO-Nb_2O_5 core/shell and aluminium doped ZnO electron transporting layer with CdS/CdSe quantum dot-sensitized solar cells

P Venkatachalam[a,b*] & S Rajalakshmi[c]

[a]Department of Physics, Annamalai University, Annamalai Nagar, Chidambaram 608 002, India

[b]Department of Physics, Periyar Arts College, Cuddalore 608 002, India

[c]Department of Physics, University College of Engineering Panruti, Panruti 607 106, India

Received 9 October 2019; accepted 11 February 2020

In the present investigation, solar cells have been fabricated using Cds/CdSe quantum dots sensitized ZnO photoanode for solar cell application. Photocurrent-voltage analysis and electrochemical impedance spectroscopy (EIS) measurements have been performed to investigate the electron transport and recombination of charge carriers in quantum dot-sensitized solar cells (QDSSCs) based on ZnO photoanodes. This dynamic study reveals that the CdS/CdSe sensitized aluminium (Al) doped ZnO NPs photoanode solar cell performs ultrafast electron transport and high charge collection efficiency (80 %). As a consequence, a power conversion efficiency as high as 5.32 % (J_{SC} = 12.86 mA/cm^2, V_{OC} = 600 mV, FF = 69 %) for aluminium doped ZnO NPs/CdS/CdSe photoelectrode based QDSSC is observed under one sun AM 1.5 G illumination (100 mW cm^{-2}). This result highlights the necessity of treating QD-sensitized solar cells from another perspective than dye sensitized solar cells, considering the fundamental differences in their behavior.

Keywords: Quantum dot solar cell, Core/shell structure, Doping, XRD, TEM, Photovoltaic, EIS

1 Introduction

Semiconductor quantum dots (QDs) afford a unique platform for designing an extensive array of optoelectronic applications due to quantum confinement and enhanced surface-to-volume ratios. These unique size-dependent properties allow for emergent electrical and optical phenomenon derived from QD−QD, and QD−ligand electronic coupling. Benefits and advantages of QDs include strong optical transitions (light absorption and emission), a huge range of tunable bandgap onset energies, control over band edge energies and work-function, facile synthesis, facile incorporation into matrices or deposition as thin films, and desirable excited state properties such as enhanced multiple exciton generation (MEG), long carrier lifetimes, and charge and energy transfer phenomenon with surface adsorbates[1].

Solar cells fabricated from QDs (QDSCs) have the potential to reveal higher power conversion efficiencies through enhanced MEG, but have not yet reached their full potential. Although MEG is enhanced in typical quasi-spherical QDs over the bulk and conventional thin film semiconductors, the threshold and efficiency of the MEG process can be improved through shape control, internal QD heterojunction interfaces, and further material exploration. Research toward increasing the MEG efficiency is an ongoing effort. However, to take advantage of these unique properties, researchers must also develop prototype energy conversion architectures that can serve as a test bed for advanced nanoscale phenomena. Incorporation of the topic of nanoparticles into the curriculum is important and becoming more prevalent. Besides their size-tunable luminescence color, their emission of light is bright and nearly monochromatic with a very narrow emission band, making them especially pleasing to the eye. Furthermore, their molar extinction coefficient is much larger than traditional organic dyes, making for strong absorbers to harness sunlight for photovoltaics, although the exact role that QDs play is still under investigation[3]. Solar cells harvest energy in the form of light, converting it to electrical energy. As the QDs are strong light absorbers, with extinction coefficients that surpass even the strongest organic absorbers, they are suitable for usage as light harvesters in dye sensitized solar cells. Among the various stuffs that are used for QDSCs,CdS,CdSe are alternative owing their high potential in light harvest

*Corresponding author (E-mail: rajalakshmiaup@gmail.com)

in the visible- light regien. When an appropriate material is placed next to the QDs, the excited QD electrons can transfer to it, resulting in a voltage when the circuit is complete. This energy transfer requires that the absorbing layer is in very close proximity to the conducting layer. Moreover, quantum dots can generate more than two electrons from a single photon when they absorb light with higher energy than the band gap of quantum dot (multiple-carrier generation). This may open up the possibility of exceeding the Schottkye Queisser limit. Nevertheless, the achieved conversion efficiencies of quantum-dot-sensitized solar cells (QDSCs) have been 5% so far[2].

The role of semiconductor porous electrode is crucial, and the cell's overall energy conversion efficiency strongly depends on the surface and electronic properties of the electrode. Until now, the DSSCs made with porous anatase TiO_2 films have represented the highest energy conversion efficiency of 11.1 %, although various oxide semiconductors, such as ZnO, have been used to prepare the porous electrode. The ZnO can be used as electrode material for the DSSCs due to its band gap (3.37 eV) and electronic properties similar to TiO_2. In addition, ZnO with flat band potential higher than TiO_2 is beneficial for enhancing the cell's open-circuit photovoltage[4,5]. In this work, ZnO NPs/Neobedium oxide core/shell structure and aluminium doped ZnO NPs photoanode film were prepared and applied in the QDSSCs.

2 Experimental

2.1 Preparation of ZnO NPs

About 4 mol/L NH_3H_2O solution was slowly dropped into the 0.5 mol/L $Zn(NO_3)_2$ solution with a speed of 3 ml/min which was initially added into a 250 ml three-necked flask, and the mixed solution was slowly stirred, and the temperature of the reaction was controlled at 60 °C. The addition of NH_3H_2O was stopped when the pH of the mixture attained pH 8.0. The mixed solution was stirred continuously for 30 min. The suspension was aged for 5 h at 70 °C, and then was filtered. The prepared sample was washed with de-ionized and ethanol for a number of times to make sure that the residual impurities was removed. The reaction yield was atmospheric-dried at 80 °C for 5 h, and then was calcined at 500 °C for 1 h in a muffle furnace with a heating rate of 5 °C/min. The obtained final product was a white powder[6].

2.2 Preparation of ZnO NPs-Nb_2O_5 core/shell structure

The Nb_2O_5 precursor solution was synthesized from a 0.02 M $NbCl_5$ solution in anhydrous ethanol. The solution was slowly dropped onto the ZnO NPs layer and spin-coated to remove the residual precursor solution. The Nb_2O_5 coating thickness was determined by the number of coatings applied. Finally, the substrate was sintered at 500 °C for 30 min to complete the conversion into a crystallized Nb_2O_5 layer[7].

2.3 Preparation of Aluminium doped ZnO NPs

A solution of Zn $(AC)_2$ (2 mmol) and $AlCl_3$ (2 mmol) in $EtOH/H_2O$ solvent (30 mL) was added to a solution of NaOH (6 mmol) in $EtOH/H_2O$ solvent (10 mL) is stirred under room temperature under stirring. After 30 min, stirring the mixture transferred into Teflon-lined stainless steel autoclaves, sealed, and maintained at 150 °C for 24 h. Subsequently, the reactor was immediately cooled down to room temperature immediately. The resulting white solid products were centrifuged, washed with distilled water and ethanol to remove the remaining ions in the final products,and finally dried at 60 °C in the air[8].

2.4 CdS QDs synthesis

CdS QDs was synthesized on the basis of the methods described by Winkler[9]. The 1800 MW polyethylenimine (PEI), $Cd(NO_3)_2 \cdot 4H_2O$, and $Na_2S \cdot 9H_2O$ solutions were made in methanol at varying concentrations and temperatures. The Cd and S sources were added in 1 mL intervals to prevent formation of large particles. The CdS QDs were cleaned of excess PEI with fresh methanol.

2.5 CdSe QDs synthesis

CdSe QDs was prepared by the basic protocol of Landry[10]. Care was taken while handling Se and $Cd(OAc)_2 \cdot 2H_2O$ in their dry state by transferring them inside a fume hood. Trioctylphosphine (TOP) was transferred to the round-bottom flask using a cannula and nitrogen atmosphere. Oleic acid was also used as a passivating agent, and octadecene, a high-boiling, nonpolar solvent, was used. The synthesis was conducted at 165 °C, and aliquots were removed from the reaction chamber over short time increments, essentially as quickly as possible starting immediately until the reaction color stabilized.

2.6 Fabrication of QDSSCs

The photoanodes were prepared using ZnO NPs, ZnO NPs/Nb_2O_5 core/shell and aluminium doped ZnO

NPs paste coated in the thickness of 10 µm by doctor blade technique on FTO glass plate (8-10 Ω/square) of an active area of 1cm^2. The photoanodes were immersed overnight in a solution of CdS/CdSe QDs. The QDs sensitized photoanode was coated with Ta_2O_5 blocking layer by dipping precursor solution, followed by sintering at 450 ºC for 20 min. The thickness of Ta_2O_5 blocking layer was controlled by dipping time and was measured by 15 nm. Four types of QDSSCs were fabricated using the QDs sensitized ZnO NPs photoanode without blocking layer (QDSSC-1), ZnO NPs/Nb_2O_5 core/shell structure without blocking layer (QDSSC-2), aluminium doped ZnO NPs with blocking layer of Ta_2O_5 (QDSSC-3), ZnO NPs/Nb_2O_5 core/shell structure with blocking layer of Ta_2O_5 (QDSSC-4). Polytriarylamine (PTAA) is used as a hole transporting materials (HTM) for all photoanodes sandwiched together with graphite coated counter electrode. The PTAA was spun coated at 2000 rpm for 30 s and the PTAA solution was prepared by dissolving 30 mg of PTAA in 1 mL of toluene, 18.8 mL of LiTFSI stock solution (170 mg of LiTFSI in 1 mL of acetonitrile) and 9.4 mL of 4-tert-butylpyridine were also added[11]. A graphite coated counter electrode was then clipped on top of the photoanode to form photovoltaic devices.

2.7 Characterization of QDSSCs

The QDSSCs were characterized by recording the photocurrent–voltage (J–V) curves under illumination of A.M. 1.5G (100 mW/cm^2). The photoanode samples were characterized by X-ray diffraction (XRD) on X'Pert PRO-PANalytical X-ray diffractometer. Morphology of the samples was recorded by transmission electron microscope (TEM) PHILIPS TECNAI10 model operated at 200 KV. The surface morphology and composition of elements presented in the photoanode sample was examined by scanning electron microscope with energy dispersive X-ray spectrometer (SEM/EDX) VEGA3SB model. Electron impedance spectra of PSSCs were recorded with potentiostat/galvanostat (Gamry-300). The applied bias voltage and ac amplitude were set at an open-circuit voltage of the PSSCs and 10 mV between working electrode and the counter electrode. The frequency range explored was 1 mHz to 10^5 Hz. The impedance spectra were analyzed by an equivalent circuit model, interpreting the characteristics of the PSSCs through Zsimpwin software.

3 Results and Discussion

3.1 XRD Analysis

The X-ray diffraction pattern of the pure ZnO NPs, aluminium doped ZnO NPs and ZnO NPs/Nb_2O_5 core/shell structure are shown in Fig. 1(a-c). From Fig. 1(a), it could be noticed that the sharp diffraction peak of pure ZnO NPs at (1 0 0), (0 0 2), (1 0 1), (1 0 2), (1 0 3), (2 0 0), (1 1 2), (2 0 1) and (2 0 2). All the diffraction peaks are well crystallized and indexed to the hexagonal ZnO wurtzite structure (JCPDS no. 36–1451). From the Fig. 1(b), it could be observed that the peaks at 34°, 36°, 43°, 47°, 56° and 62° corresponds to the planes respectively (8 0 0), (8 2 0),

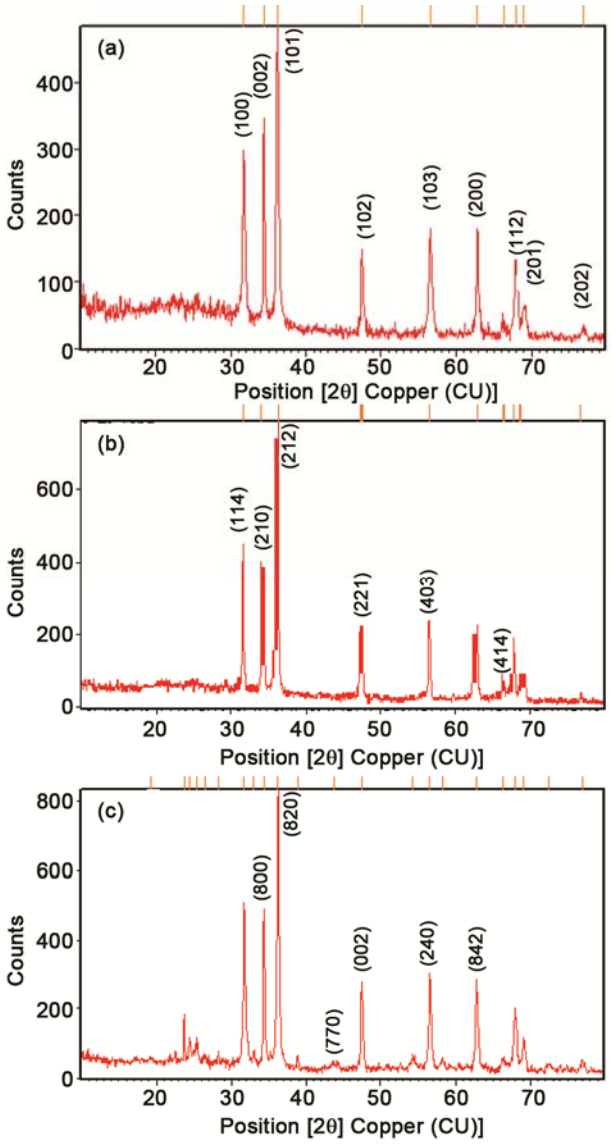

Fig. 1 — XRD pattern of (a) ZnO NPs, (b) Al doped ZnO NPs and (c) core/shell Nb_2O_5-ZnO NPs.

(7 7 0), (0 0 2), (12 4 0) and (8 4 2) of Nb_2O_5 phase (JCPDS card No. 72-1484). From the Fig. 1(c), the peaks at 35°, 43°, 52° and 57° are indexed to the Al phase[12]. From the XRD results, the diffraction peaks confirming the high purity of the synthesized products.

3.2 Microstructural analysis

The TEM image of ZnO NPs, aluminium doped ZnO NPs and core/shell ZnO NPs/Nb_2O_5 were shown Figs 2(a), 2(b) and 2(c) respectively. The image illustrates ZnO nanoparticles are spherical in shape with smooth surface and the size of the particles around 20-50 nm. From the Fig. 2(a), it can be seen that the average size of the nanoparticles is 50 nm which is in good agreement with the particle size calculated from the Debye-Scherrer formula of XRD pattern. Fig. 2(b) indicates that the structure of the aluminium doped ZnO NPs, which are spherical in size with the diameter varying between 10 to 30 nm. This implies that the particle is smaller in size as compared to the pure ZnO NPs. The results are in good agreement with the XRD pattern. From the Fig. 2(c), the core/shell ZnO NPs/Nb_2O_5 exhibits the spherical in nature with smooth surface.

3.3 J-V analysis

The light conversion properties of QDSSCs based on these four photoelectrodes (ZnO NPs, ZnO NPs/Nb_2O_5, aluminium doped ZnO NPs /Ta_2O_5 and ZnO NPs/Nb_2O_5/Ta_2O_5) were characterized as current density-voltage curves (J-V, shown in Fig. 3), while the details of short circuit current density (J_{SC}), open circuit voltage (V_{OC}), fill factor (FF) and power conversion efficiency (η) are listed in Table 1. The ZnO NPs QDSSC shows the lowest J_{SC} and η due to the poor light absorption in a narrow region. The J_{SC} increases obviously for aluminium doped ZnO NPs/Ta_2O_5 and ZnO NPs/Nb_2O_5/Ta_2O_5 QDSSCs, accompanied by an apparent enhancement of FF value. As a result, the power conversion efficiency more than doubled for QDSSC-3, while an outstanding η of 5.32 % was observed for aluminium doped ZnO NPs/Ta_2O_5 photoanode under one sun illumination (100 mW/cm^2). From the Table 1, it could be observed that QDSSC-3 shows highest PCE as compared to other QDSSCs, and had the photovoltaic parameters Voc = 600 mV, Jsc = 12.86 mA/cm^2, FF = 69 % and η = 5.32 %. This enhancement (22%) of PCE might be due to the Al doping in QDSSC-3 when compared to the QDSSC-4. The photovoltaic parameters of QDSSC-4 are V_{OC} = 620 mV, J_{SC} = 11.12 mA/cm^2, FF = 63 % and η = 4.34 %. The photovoltaic parameters of QDSSC-1 are V_{OC} = 560 mV, J_{SC} = 4.84 mA/cm^2, FF = 54 % and η = 1.46 %. When comparing QDSSC-1 and QDSSC-3, the later shows the enhanced PCE due to plasmonic effect. Doping of metal ions in ZnO is the area of research for the scientist and researchers. One of the significant applications of this doping is the solar cells with plasmonic effect. Aluminium doping plays a vital role in increasing solar cell performance. To increase the light harvesting of dye sensitized solar

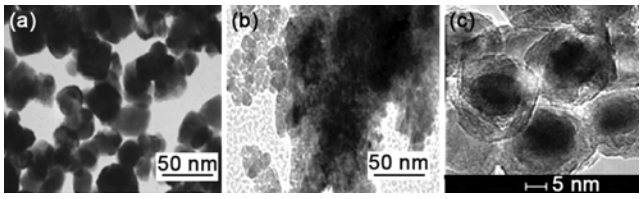

Fig. 2 — TEM image of (a) ZnO NPs, (b) Al doped ZnO NPs and (c) Core/shell Nb_2O_5-ZnO NPs.

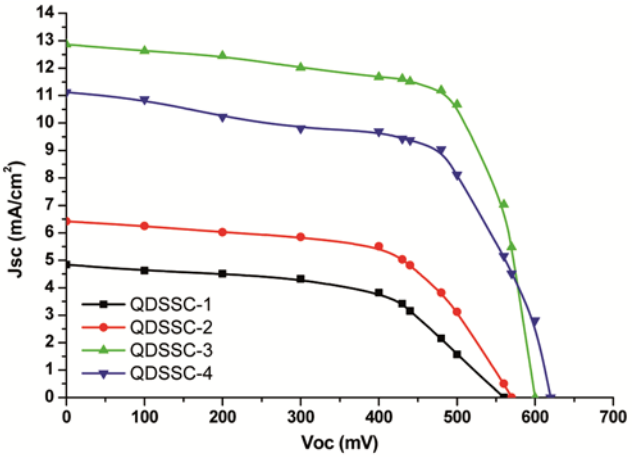

Fig. 3 — J-V curves of QDSSCs.

Table 1 — J-V and EIS values of QDSSCs.

QDSSCs	Voc (mV)	Jsc (mA/cm^2)	FF (%)	η (%)	R_{tr} Ω	R_{rec} Ω	C_{rec} mF	τ_n ms	L_n µm	$D_{eff}\times10^{-6}$ cm^2/s	µ × 10^{-5} cm^2/V/s	σ ×10^{-5} S/cm	Conc. Ω cms^{-1}	η_{cc} (%)
QDSSC-1	560	4.84	54	1.46	32	42	4.82	202	1146	6.48	25.22	4.46	0.21	23
QDSSC-2	570	6.42	58	2.12	26	52	5.32	277	1414	7.23	28.12	6.41	0.19	50
QDSSC-3	600	12.86	69	5.32	18	92	6.42	591	2261	8.65	33.66	13.89	0.16	80
QDSSC-4	620	11.12	63	4.34	16	72	7.84	564	2121	7.97	31.01	15.25	0.13	77

cell (DSSCs), surface plasmon resonance effect of metal nanoparticles may be incorporated in photoanode. The results show that these metal nanoparticles may localize the incident light and extend the optical path length in QDSSCs for the improved performance[13,14]. The improved PCE in the QDSSC-2 made with aluminium doped ZnO NPs photoanode is attributed to the plasmonic effect introduced by the Al nanoparticles. When Al nanoparticles located on dielectric surfaces are illuminated with light, a greatly enhanced electromagnetic field occurs near the Al nanoparticle surface, if the light wavelength resonates with the electron plasma frequency. As is well known, the magnitude of the plasmon enhancement effect is closely related to the relative position between the Al nanoparticle and the sensitizer molecules, and the light–matter interaction is stronger for smaller relative distances[15]. Therefore, the strongly localized electromagnetic field around the Al nanoparticles will strongly enhance the optical absorption efficiency of the sensitizer molecules, resulting leads to increased PCE in DSSC-3. The reason for the photocurrent enhancement may be ascribed to the fast electron transfer rate in the aluminium doped ZnO NPs photoanode. First, Al nanoparticles and ZnO NPs forms a Schottky contact, which favours electron transfer in the photoanode.

From the PV values of QDSSC-1 and QDSSC-2, it could be observed that the core/shell structure increases the performance (45 %) of the device due to the more specific surface of ZnO NPs/Nb_2O_5. The higher specific surface area of ZnO NPs/Nb_2O_5 core/shell structure could lead to adsorb more sensitizer molecules on the surface of the photoanode hence the increase of the PCE in QDSSC-2. The improvement of the PCE of the devices QDSSC-3 and QDSSC-4 is ascribed to the increase of the J_{SC} and V_{OC}. Two possible mechanisms intended for the increased J_{SC} and V_{OC}. They are blocking effects and surface dipole effects[16]. QDSSCs fabricated with Nb_2O_5 layer photoanode had a higher conduction band edge, the shell layer act as blocking barrier for their combination of the injected electrons either with the oxidized sensitizer molecules or with the HTM. The improved photocurrent density of QDSSC-4 had illustrated that the charge recombination has been retarded by the Nb_2O_5 layer at photoanode/ sensitizer/HTM interface. If their combination of the injected electrons is retarded, the electron population and the resulting quasi Fermi level of photoanode near the shell layer could be increased[17]. As a result, the V_{OC} is increased due to the increased off set between the quasi Fermi level of photoanode and the HTM. This is the "blocking effect" of the shell layer [16]. The shell layer induced the positive charges on the surface, and an electrostatic field is generated, which could increase the off set of conduction edges. This is surface dipole effects, this increases the V_{OC}.

The photovoltaic parameters of QDSSC-2 are V_{OC} = 570 mV, J_{SC} = 6.42 mA/cm^2, FF = 58 % and η = 2.12 %. When comparing QDSSC-2 and QDSSC-4, the PCE is increased 104 % in QDSSC-4 because of the Ta_2O_5 blocking layer. From the PCE values of QDSSC-3 and QDSSC-4, it could be noticed that the Ta_2O_5 blocking layer/scattering layer improved the PCE. The introduction of thin Ta_2O_5 layer apparently decreased their combination rate of the photo injected electrons with the oxidized sensitizer or ions in the HTM by forming an energy barrier. The Ta_2O_5 layer over the dye sensitized photoanode film significantly improved the PCE. The improvement of the J_{SC} is mainly due to the enhanced necking property of blocking layer at photoanode film/Ta_2O_5 and the reduced electron recombination. The PTAA is one of the widely used organic hole conductor. This solid electrolyte has small molecular size, high solubility and amorphous structure, which make it suitable in the impregnation into mesopores. In addition, the redox potential of the PTAA is more positive than that of the I^-/I_3^- couple, which is beneficial in increasing V_{OC} of QDSSCs. Hereby, we conclude that J_{SC} and η of QDSSCs are affected by three factors: (i) light absorption intensity determined by both the QD material and the amount of loading; (ii) electron transport influenced by the band edge position and electron concentration; (iii) charge recombination rate.

3.4 EIS analysis

Electrochemical impedance spectroscopy (EIS) is further utilized to investigate the recombination processes of QDSSCs based on the four photoelectrodes. Furthermore, using the EIS internal resistances and the electron transport kinetics of the QDSSCs was also studied. Figure 4 shows the Nyquist plots of the electrochemical impedance spectra of the QDSSCs measured under 100 mW/cm^2 and the equivalent circuit is shown as the inset of Fig. 5. Generally, the Nyquist plot of

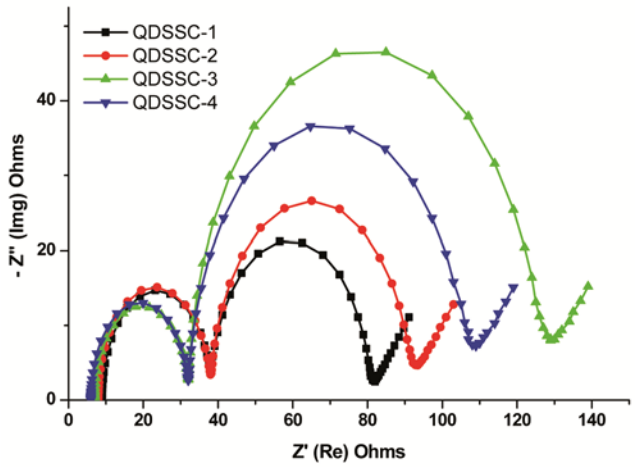

Fig. 4 — Nyquist plots of QDSSCs.

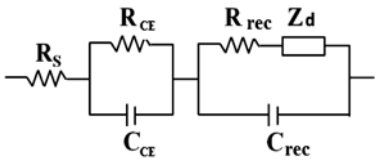

Fig. 5 — EIS equivalent circuit diagram.

electrochemical solar cell devices exhibited three semicircles, which are assigned to electrochemical reaction at the counter electrode, charge transfer at the photoanode/sensitizer/HTM and Warburg diffusion process. In the present study, the equivalent circuit consists of series resistance (R_s, starting point of the first semicircle in Nyquist plot), electron transport resistance at the counter electrode/HTM (R_{CE}, first semicircle in Nyquist plot), recombination resistance (R_{rec}) at the photoanode/sensitizer/HTM (second semicircle in Nyquist plot), the constant phase elements of capacitance C_{rec} (R_{rec}), C_{CE} (R_{CE}) and Warburg diffusion impedance Z_d. The other useful electrochemical parameters of QDSSCs are τ_n (electron life time), L_n (electron diffusion length), D_{eff} (effective diffusion coefficient), μ (electron mobility), σ (electron conductivity), η_{cc} (electron collection efficiency) and Conc. (concentration of electrons at the TiO_2/sensitizer/HTM interface) were calculated[18] and presented in Table 1.

The Nyquist plots of QDSSCs in Fig. 4, comparing the diameter of middle semicircle increased in the order QDSSC-1<QDSSC-2 <QDSSC-4<QDSSC-3, suggested that QDSSC-3 contributed a highest charge transfer resistance (R_{rec}) at the photoanode/sensitizer/HTM interface. From Table 1, it could be noticed that the higher η_{cc} is achieved in QDSSC-3 based on CdS/CdSe sensitized photoanode (aluminium doped ZnO NPs) with PTTA HTM as compared to the other devices. The PSSC-3 exhibited higher values of R_{rec}, C_{rec}, τ_n, L_n, D_{eff}, μ, σ and η_{cc} among QDSSCs. On the other hand R_{tr} and Conc. of electrons at the photoanode/perovskite interface are lower values as compared to other QDSSCs. The EIS is a useful technique for the analysis of electronic and ionic transport processes in an electrochemical device. It is a steady state method measuring the current response based on the application of an ac voltage at different frequencies[19].

Figure 4 shows the Nyquist curves of the EIS results containing typically two semicircles which are fitted by the equivalent circuit (Fig. 5) with the fitted values listed in Table 1, where the electron lifetime can be estimated by above mentioned equation. From the Table 1, it could be observed that the electron transport resistance (R_{tr}) at the photoanode/sensitizer interface is lower for QDSSC-4 and QDSSC-3 than that of other devices, ascribed to the fast electron transfer. At the photoanode/sensitizer/HTM interface (the second semicircle), the recombination resistance (R_{rec}) exhibits higher for QDSSC-3 among the other three QDSSCs; however, the value of chemical capacitance (C_{rec}) of QDSSC-4 is larger. As a result, the electron lifetime τ_n of the QDSSC-3 and QDSSC-4 calculated by EIS showed the 591 ms and 564 ms respectively indicate the lower recombination rate and higher charge transport at the photoanode/sensitizer/HTM interface of QDSSC-3.

For the efficient operation of QDSSCs, recombination pathways occurring at the photoanode/sensitizer/HTM interface should also be minimized. The generated electrons are able to recombine either with oxidized QDs or HTM. In order to reduce these backward reactions, the passivation layer (Nb_2O_5 shell layer or Ta_2O_5 blocking layer) should have a wide band gap and conduction band edge above that of ZnO NPs. At the same time, the surface charge of passivation layer is also important for the attachment of sensitizer. Considering electrostatic interactions between the sensitizer and the passivation layer makes several metal oxides more charming, because they bear more positive surface charges than ZnO NPs. In the present investigation, the suppressed charge recombination at the photoanode/sensitizer/HTM interface was analyzed by the EIS analysis indicates that the recombination between electrons in that interface is drastically reduced by the compact aluminium doped ZnO NPs/Ta_2O_5 and ZnO NPs/Nb_2O_5/Ta_2O_5 layer. Also, it could be observed

from the EIS results, electron-carrier lifetime of the QDSSC-3 is approximately three times higher compared with the QDSSC-1. In addition, the increase in efficiency is likely to arise from an abundant adsorption of QDs sensitizer, and reduced carrier recombination at the photoanode/sensitizer/ HTM interface. Another approach to minimize leakage electrons at photoanode/sensitizer/HTM interface is to introduce potential-barrier layer/ scattering layer such as Ta_2O_5. The metal oxide blocking layer can remarkably decrease the charge recombination, resulting in higher Voc and Jsc (QDSSC-4) compared with the QDSSC-2.

As shown in Table 1, the optimized shell layer (QDSSC-2) enhances the power-conversion efficiency by 45 % compared with the QDSSC-1. The enhanced efficiency by the shell layer on the ZnO NPs electrode is attributed to the reduction of charge recombination at the photoanode/sensitizer/HTM interfaces by passivating the surface defects on the ZnO NPs layer. The effective suppression of recombination was confirmed by impedance analysis at the open-circuit voltage under AM 1.5 illumination. The recombination resistance (R_{rec} = 72 ohms) shows higher values, which means that the Nb_2O_5 coating layer effectively suppresses charge recombination at the photoanode/sensitizer/HTM interface. The light harvesting properties can also be amplified by employing surface-plasmon resonance. Surface plasmons are created when incident light excites oscillations of free electrons in metal nanoparticles, such as gold, aluminium, and silver. Hupp's group investigated the plasmon-enhanced absorption of the dyes by introducing silver nanoparticles [20]. In this study, the QDSSC-3 shows highest PCE and charge collection efficiency due to the plasmonic effect. These results clearly confirm that spectra overlap between the sensitizer and surface plasmon can give rise to an effective light absorption by the field-enhancement effect.

The J-V and EIS results revealed that the electron transport rate in the devices follows the order of QDSSC-3>QDSSC-4>QDSSC-2>QDSSC-1. The results illustrated as a consequence of the following facts: (i) The higher intensity and red shift of light absorption in 400-750 nm increase the electron concentration in the photoanode substrate of QDSSC-3 and QDSSC-4 compared to QDSSC-1, which directly accelerates the electron transport in ZnO NPs and transfers to FTO glass. (ii) In the present QDSSCs with HTM, the Al doped ZnO NPs/CdS-CdSe and ZnO NPs/Nb_2O_5/CdS-CdSe structure can provide a larger driving force for photogenerated electron injection than the ZnO NPs/CdS-CdSe structure. Although the conduction band (CB) energies of CdS and CdSe are 0.8 V and 0.6 V As a result, when compared to CdS QDs, the more negative conductive band energy level of CdSe QDs offers a larger driving force for electron transfer to the HTS substrate. (iii) Because of the band edge shift in the HTM, the photoanode/CdS/CdSe cosensitized solar cell with step-like band edge structure is more efficient in enlarging the charge separation. In other words, the shunting of the electrons and holes in different directions accelerates the electron transport in the photoanode [21]. Furthermore, the aluminium doped ZnO NPs/CdS-CdSe and ZnO NPs/Nb_2O_5/ CdS-CdSe structure allows electron transport without obstruction in a certain range, which provides an important factor in the fast electron transit in the QDSSCs.

4 Conclusions

In the present work, it could be concluded that the PCE of QDSSCs is in the order of QDSSC-3>QDSSC-4>QDSSC-2 >QDSSC-1. The EIS measurement shows a high charge collection efficiency of 80 % and 77 % for QDSSC-3 and QDSSC-4 respectively. Moreover, for QDSSC-3, higher light harvesting efficiency caused by strong light absorption and better electron injection efficiency ascribed to step-like band gap structure lead to an outstanding η of 5.32 %, which is much higher than that of QDSSC-1 (1.46 %) and QDSSC-2 (2.12 %). The development of near IR absorption QDs and efficient photoanode (core/shell or doping structure) would be expected to enhance the photovoltaic performance of QDSSCs significantly. This highly efficient hybrid sensitization was demonstrated as a promising alternative to conventional organic dye sensitized solar cells, with significant potential advantages enabling broader absorption spectra with an increased choice of the sensitizers, and excluding elaboration of simultaneous stability of the sensitizers. Besides, such a scheme is compatible with the use of alternative electrolytes such as PTAA electrolyte, which has exhibited outstanding photovoltaic performances and also high stability in QD sensitized solar cell and is expected to contribute to the long term stability of such systems. Further research work on the elucidation of such fundamental issues is now underway.

References

1 Chernomordik D B, Marshall R A, Pach F G, Luther M J & Beard C M, *Chem Mater*, 29 (2017) 189.

2 Choi H, Changwoo N, Jongmin K, Chohui K, Suji K, Taehyun H & Byungwoo P, *Curr Appl Phys*, 13 (2013) S2.

3 Bauer C A, Hamada T Y, Kim H, Johnson M R, Voegtle M J & Emrick M, *J Chem Edu*, 95 (2018) 1179.

4 Nuhad A A, Reda M S & Al-Hajri M F, *Adv Nanopart*, 3 (2014) 31.

5 Kumar R, Umar A, Kumar G, Nalwa H S, Kumar A & Akhtar M S, *J Mater Sci*, 4743 (2017) 52.

6 Tsai C Y, Kuo T H & His H C, *Int J Photoenergy*, Article ID 874509, (2012).

7 Maheswari D & Venkatachalam P, *Photon Nanostruct Fund Appl*, 12 (2014) 515.

8 Zamani E, Fatemeh R, Sara B, Mahdieh G, Maryam M, Saeid F, Abedin Z & Alireza A, *Int J Nano Chem*, 1 (2015) 19.

9 Winkler L, Arceo J F, Hughes W C, DeGraff B A & Augustine B H, *J Chem Edu*, 82 (2005) 1700.

10 Landry M, Thomas M E, Theodora K K, Chih-Hao H & Chia-Ying W, *J Chem Edu*, 91 (2013) 274.

11 Ramos J F, Maria L S C, Elena Gu, Mohammad K N, Michael G, Agustin G E R & Shahzada A, *Chem Phys Chem*, 15 (2014) 1148.

12 Manoharan K & Venkatachalam P, *Mater Sci Semicond Proc*, 30 (2015) 208.

13 Chen P Y, Xiangnan D, T Matthew K, Jifa Q, Noémie-Manuelle D C, Burpo J F, Nicholas F, Hammond T P & Angela B M, *ACS Nano*, 7 (2013) 6563.

14 García de A, Pelayo F, Agustín M, Dominik K & Gerasimos K, *ACS Nano*, 7 (2013) 3581.

15 Standridge S D, George S C & Joseph H T, *Langmuir*, 25 (2009) 2596.

16 Hara K, Mitsuhiko K, Yasufumi D O, Chiaki K, Akira S, Sadaharu S, Kazuhiro S & Hironori A, *New J Chem*, 27 (2003) 783.

17 Wu J J, Chen G R, Lu C C, Wu W T & Chen J S, *Nanotech*, 19 (2008) 105702.

18 Ramavenkateswari K & Venkatachalam P, *Electron Mater Lett*, 12 (2016) 628.

19 Ross M J, William K R, *Impedance Spectroscopy, Emphasizing Solid Materials and Systems*, Wiley, New York (1987).

20 Standridge S, George S C & Joseph H T, *J Am Chem Soc*, 131 (2009) 8407.

21 Yu X Y, Liao J Y, K Q Qiu, Kuang D B & Su C Y, *ACS Nano*, 5 (2011) 9494.